Chinese Chemical Letters 33 (2022) 3713–3720

Contents lists available at ScienceDirect

Chinese Chemical Letters

journal homepage: www.elsevier.com/locate/cclet

$CoFe_2O_4$ nanoparticles anchored on waste eggshell for catalytic oxidation of florfenicol *via* activating peroxymonosulfate

Yingjie Gao[a], Ying Han[a], Bingrui Liu[a], Jianfeng Gou[a], Dan Feng[b,c], Xiuwen Cheng[a,b,c,*]

[a] *Key Laboratory for Environmental Pollution Prediction and Control, College of Earth and Environmental Sciences, Lanzhou University, Lanzhou 730000, China*

[b] *College of Chemistry and Environmental Sciences, Yili Normal University, Yining 835000, China*

[c] *Key Laboratory of Pollutant Chemistry and Environmental Treatment, Yili Normal University, Yining 835000, China*

ARTICLE INFO

Article history:
Received 26 August 2021
Revised 7 October 2021
Accepted 30 November 2021
Available online 5 December 2021

Keywords:
$CoFe_2O_4$/eggshell
Peroxymonosulfate
Florfenicol
PVDF membrane

ABSTRACT

Eggshell-loaded $CoFe_2O_4$ catalyst was synthesized *via* a convenient hydrothermal method during our work, then the surface morphology and elemental composition of the composites were systematically investigated. Performance of $CoFe_2O_4$/eggshell-activated peroxymonosulfate (PMS) system was evaluated by selecting florfenicol (FF) as the model pollutant, and effects of operating parameters and water matrices on the FF removal efficiency in this system were investigated. In addition, main radicals involved in FF degradation were identified by EPR tests and radical quenching experiments, and possible mechanism was proposed. The reduction of toxicity during FF degradation was confirmed, and in combination with HP-LC tests, it was found that dehalogenation and defluorination were effectively carried out during FF degradation. In addition, the prepared $CoFe_2O_4$ polyvinylidene fluoride (PVDF) membrane effectively improved the stability of the material and reduced the precipitation of metals.

Florfenicol (FF) was successfully developed in the late 1980s as a new broad-spectrum antibiotic of chloramphenicol for veterinary use. It was estimated that more than half of antibiotic drugs failed to be absorbed by animal gut. Subsequently, unabsorbed antibiotics were likely released into the water environment through livestock animals' feces [1]. The presence of antibiotics in water environment would produce new antibiotic-resistant bacteria and genes, which could adversely affect ecology and human health.

Advanced oxidation processes (AOPs) may provide effective elimination methods of antibiotics. Due to the high oxidative potential of hydroxyl radical ($^{\bullet}OH$) generated during these processes, bio-refractory antibiotics could be decomposed into harmless products [2]. Jiang *et al.* successfully fabricated a novel electro-Fenton membrane modified by graphene for low-concentration FF's *in-situ* elimination [3]. Liu *et al.* group reported the photodegradation of FF through UV irradiation, UV/H_2O_2 and UV/Fe(II) system [4]. Among AOPs, sulfate radical ($SO_4^{\bullet-}$) based AOPs (SR-AOPs) can produce $SO_4^{\bullet-}$ for oxidizing most antibiotic pollutants without restriction to specific classes or groups of compounds [5]. Compared with $^{\bullet}OH$, $SO_4^{\bullet-}$ has the advantages of higher standard reduction potential, longer half-life, and higher reaction stoichiometric efficiency [6].

Activating persulfate (PS) or peroxymonosulfate (PMS) through various means [6] is the most common method to generate $SO_4^{\bullet-}$. Compared with PS, PMS is easier to be activated because of it is relatively less stable molecular structure (*i.e.*, PS is symmetrical and PMS is asymmetrical) and lower bond dissociation energies [7]. In previous studies, Anipsitakis and Dionysiou pointed out that Co^{2+} exhibited the highest PMS activation activity to produce $SO_4^{\bullet-}$ [8], while the dissolved cobalt may cause secondary pollution due to its aqueous toxicity. Shih *et al.* stated that materials with the general formula of AB_2X_4 structure could substantially immobilize metal ions and reduce metal leaching rate [9]. On account of its surface activity and ferromagnetic property [10], the spinel cobalt ferrite nanoparticles ($CoFe_2O_4$) exhibited expected performance in $CoFe_2O_4$ and PMS system. However, because of strong magnetic property and great surface energy [11], $CoFe_2O_4$ nanoparticles would agglomerate with each other extensively in solution to form spherical aggregates, which greatly decrease their catalytic oxidation efficiency [12]. To overcome this phenomenon, Tan et al. utilized natural diatomite to mediate spherically monodispersed $CoFe_2O_4$ nanoparticles to elevate catalytic efficiency [13]. Li *et al.* used drinking water treatment residuals (WTRs) as the

* Corresponding author at: Key Laboratory for Environmental Pollution Prediction and Control, College of Earth and Environmental Sciences, Lanzhou University, Lanzhou 730000, China.
E-mail address: chengxw@lzu.edu.cn (X. Cheng).

https://doi.org/10.1016/j.cclet.2021.11.096
1001-8417/

catalyst carriers to improve the dispersion of $CoFe_2O_4$ [14]. Other measures, such as dispersing $CoFe_2O_4$ on biochar [15], montmorillonite [16] and other carrier materials to improve the catalytic activity.

The global annual output of eggshell is more than 50,000 tons, which produces a lot of waste. Due to its magical ordered structure, eggshell, a unique natural biomaterial, can achieve a higher surface area with fewer materials [17]. Different layers are deposited around the protein of the last segment of the hen's oviduct, and polycrystalline tissue is formed around the calcified eggshell, which leads to the formation of many funnel-shaped pores on the surface of the eggshell, which can provide a perfect biological platform for nanoparticles [18].

Herein, for the first time, the synthesis of $CoFe_2O_4$ nanoparticles anchored on the surface of eggshell ($CoFe_2O_4$/eggshell) was reported. In order to reduce metal dissolution from powder $CoFe_2O_4$/eggshell, corresponding polyvinylidene fluoride (PVDF) membrane had been synthesized. Moreover, the catalytic mechanism and degradation pathway were clarified.

The eggshells were collected in Danguiyuan canteen of Lanzhou University, washed by ultra-pure water repeatedly, and then dried and grounded into powder. More details of the materials and synthesis method of $CoFe_2O_4$/eggshell and PVDF membrane could be found in Text S1 (Supporting information). For details on the characterization of materials and degradation experiment, see Text S2 (Supporting information). The details about the method to character the PMS consumption were presented in Text S3 (Supporting information), and the method to measure the biological toxicity during the FF degradation was observed *via* activated sludge inhibition experiment, which was described in Text S4 (Supporting information).

Pure eggshell, Co_3O_4, Fe_2O_3, $CoFe_2O_4$, and $CoFe_2O_4$/eggshell composite samples were tested and characterized using X-ray diffraction (XRD) analysis method, and data were presented in Fig. S2 (Supporting information). According to the standard cards shown in Fig. S2b, pure eggshell, Co_3O_4, Fe_2O_3, and $CoFe_2O_4$ are all able to be matched with $CaCO_3$ (calcite, JCPDS PDF #86–2334), Co_3O_4 (cobalt oxide, JCPDS PDF #74–2120), Fe_2O_3 (iron oxide, JCPDS PDF #72–0469), and $CoFe_2O_4$ (cobalt-iron oxide, JCPDS PDF #03–0864) on standard cards. Notably, diffraction peaks at 23.059°, 29.404°, 35.980°, 39.419°, 43.171°, 47.508° and 57.416° were observed in $CoFe_2O_4$/eggshell composites, which are indexed to (012), (104), (110), (113), (202), (018), (122) and (208) planes of $CaCO_3$ (calcite, JCPDS PDF #86–2334) standard card, while peaks at 18.239°, 30.063°, 35.451°, 43.472°, 57.166°, and 62.726° can be matched to the (111), (220), (311), (400), (511), and (440) planes of $CoFe_2O_4$ [19]. This indicated that $CoFe_2O_4$ nanoparticles had been successfully loaded on the eggshell surface.

To further study the morphology of pure eggshell and $CoFe_2O_4$/eggshell catalyst, SEM tests of which were recorded. SEM analysis of pure eggshell, which exhibited in Figs. 1a and b, revealed that it is typically porous structure with certain roughness. This rough porous structure would be favorable for the stable anchoring and uniform of $CoFe_2O_4$ nanoparticles and also provide small molecular and electrolyte accesses [20]. Figs. 1c and d showed that pure $CoFe_2O_4$ nanoparticles would usually present irregular large block structure. From SEM images of eggshell supported $CoFe_2O_4$ nanoparticles (Figs. 1e and f), it could be observed that the surface of eggshell became rough, which indicated the successful immobilization and distribution of $CoFe_2O_4$ nanoparticles on eggshell surface. Meanwhile, we could also observe that when $CoFe_2O_4$ nanoparticles were loaded on eggshell, the size and agglomeration of $CoFe_2O_4$ nanoparticles would be controlled, and they could irregularly distribute on the eggshell surface and pores, no longer present a large block structure or agglomeration phenomenon, which would be conducive to the electron transfer between $CoFe_2O_4$ and PMS and further degradation of pollutants.

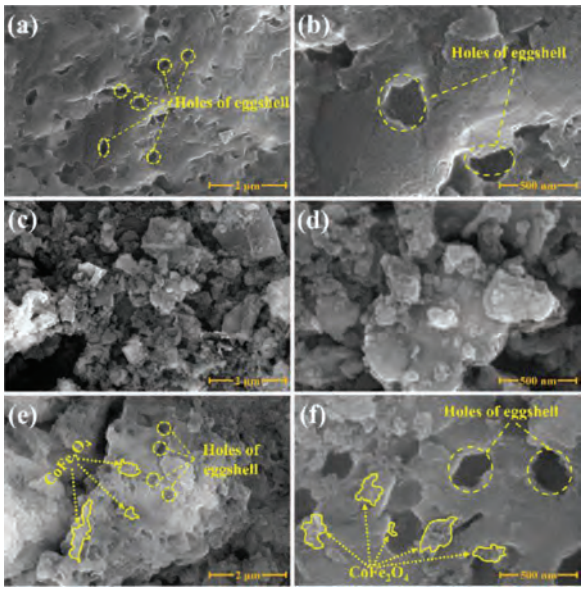

Fig. 1. SEM images of eggshell (a, b), $CoFe_2O_4$ (c, d), $CoFe_2O_4$/eggshell (40%) catalysts (e, f).

Transmission electron microscopy (TEM) was also utilized to characterize the composite samples, so as to further investigate morphology of the composite materials. The images are shown in Fig. S3 (Supporting information). The lattice fringes with the spacing of 0.486 nm could correspond to the (111) crystal plane of $CoFe_2O_4$, while the lattice fringes with the spacing of 0.294 nm and 0.255 nm could be attributed to the (220) and (311) crystal planes of $CoFe_2O_4$ crystal structure [21], respectively. Meanwhile, lattice fringes with a spacing of 0.302 nm were detected, which could match with the (104) crystal plane of $CaCO_3$ [22].

X-ray photoelectron spectroscopy (XPS) method was further applied on prepared $CoFe_2O_4$/eggshell catalysts to obtain more detailed composition of elemental species and chemical valence states of elements, and XPS analysis data are shown in Fig. S4 (Supporting information). The fine spectrum of C 1s of $CoFe_2O_4$/eggshell catalyst was exhibited in Fig. S4a, where the characteristic peak at 286.78 eV could be attributed to CO_3^{2-}, which originated from eggshell component, while the characteristic peak at 285.00 eV could originate from the exogenous carbon used for calibration of the instrument. As shown in Fig. S4b, the O 1s fine spectrum contained two characteristic peaks, the one at 530.25 eV and the one at 532.4 eV representing the lattice oxygen in catalyst and the oxygen or hydroxyl substances adsorbed on material surface, respectively [23]. Fig. S4c illustrated the Ca 2p fine spectra, from which two peaks had been detected, peaks at 348.22 eV and 351.14 eV indicating Ca $2p_{3/2}$ and Ca $2p_{1/2}$ hybridization from CaO [24,25] in $CoFe_2O_4$/eggshell composites, respectively. The fine spectra of Fe 2p were exhibited in Fig. S4d, where six characteristic peaks were observed. Two of the peaks located at 717.88 eV and 732.87 eV are satellite peaks, while the two characteristic peaks at 710.81 eV and 712.80 eV are Fe $2p_{3/2}$ hybridization, while the two peaks at 724.43 eV and 727.31 eV are Fe $2p_{1/2}$ hybridization [23]. And two peaks with binding energies at 710.81 eV and 712.80 eV could be allocated to Fe(II) and Fe(III), respectively [26]. Fig. S4e displayed the XPS spectra of Co 2p in $CoFe_2O_4$/eggshell composites, where the two main signal peaks of Co $2p_{3/2}$ (780.51 eV) and Co $2p_{1/2}$ (796.20 eV) could be observed. A series of peaks could be isolated by analytical fitting with XPS-

PEAK software, and two peaks with binding energies of 780.38 eV and 795.67 eV represented Co(III) of Co $2p_{3/2}$ and Co $2p_{1/2}$, while peaks with binding energies located at 781.58 eV and 796.79 eV could correspond with Co(II) [26,27].

In addition, to analyze surface functional groups and molecular structure of $CoFe_2O_4$/eggshell composites, FT-IR tests were conducted in this study, and data are exhibited in Fig. S5a (Supporting information). The characteristic peaks located near 3411.5 cm^{-1} and 3421.1 cm^{-1} could because of stretch vibration originated from –OH in water molecules adsorbed on the catalyst surface [28], and several weak peaks located near 2978.7 cm^{-1}–2972.4 cm^{-1} could represent the C=O functional group from carbonate [29] and C–H stretching vibration [30]. While the characteristic peaks located at 2516.7–2518.0 cm^{-1} revealed the presence of $CaCO_3$ in the composites [29]. The small spectral bands at 1796.6 and 1799.1 cm^{-1} might originate from C = O stretching vibrations [31]. The presence of calcite in $CoFe_2O_4$/eggshell catalyst could be revealed by the characteristic peaks appearing around 712.1–712.5 cm^{-1}, 874.9 cm^{-1}–875.8 cm^{-1}, and 1422 cm^{-1} [31]. Notably, compared with FT-IR spectrum of eggshell, spectrogram of $CoFe_2O_4$/eggshell composites had two additional characteristic peaks, namely those observed at 564.3 and 449.8 cm^{-1}, which could represent Fe–O and Co–O stretching vibrations, respectively [13]. And the characteristic peak situated in 611.4 cm^{-1} in the spectrogram of the eggshell confirmed the presence of C–S bonds [32], which were mainly derived from the proteins in the eggshell. And according to Nasrollahzadeh *et al.* [33], during the synthesis of composite catalytic materials, strong bonding interactions between metal and protein could effectively control the size and distribution of metal nanoparticles.

In this study, magnetic hysteresis loops of synthesized $CoFe_2O_4$/eggshell composite were detected using a vibrating sample magnetometer (VSM), which was under an applied magnetic field varying from −20 kOe to +20 kOe, and results are shown in Fig. S5b (Supporting information). The M–H curves behaviors illustrated that the $CoFe_2O_4$/eggshell catalysts exhibited superparamagnetic properties with the saturation magnetization (Ms) value of 34.505 emu/g. Furthermore, the $CoFe_2O_4$/eggshell composites could be effectively separated by applying a magnetic field after dispersion into aqueous solutions, as shown in Fig. S5c (Supporting information). Both phenomena indicated that the prepared materials had strong magnetic properties, which could be beneficial for the recycling of catalysts during the water treatment process. Meanwhile, specific surface area of eggshell and $CoFe_2O_4$/eggshell composites was explored by taking the N_2 adsorption-desorption method. Apparently, compared with the eggshell with a specific surface area of 3.1129 m^2/g, $CoFe_2O_4$/eggshell composites presented a slightly smaller specific surface area of 2.2214 m^2/g, which demonstrated that the eggshell surface and pores were loaded with $CoFe_2O_4$ nanoparticles.

To investigate heterogeneous catalytic performance, florfenicol (FF) was chosen as a targeted contaminant. The concentration of FF was monitored by HPLC, and corresponding standard curve of concentration versus instrumental response values for FF was exhibited in Fig. S6 (Supporting information).

In this study, adsorption effect of eggshell, $CoFe_2O_4$, and $CoFe_2O_4$/eggshell composites on FF was firstly investigated, and it was found that adsorption of FF by these three materials was not significant (all less than 6%). Therefore, the adsorption effect could be negligible. Meanwhile, experiments were also conducted to test the FF removal efficiency by PMS alone and eggshell-activated PMS system and the results revealed that PMS alone was not able to degrade FF (less than 2% in 40 min), and eggshell-activated PMS system was not effective in degrading FF (12.7% in 40 min), either. $CoFe_2O_4$/eggshell composites with different eggshell contents were prepared by hydrothermal method and their efficiency of activating PMS to degrade FF was compared by degradation experiments, and results were shown in Fig. S7a (Supporting information). It could be observed that $CoFe_2O_4$ could effectively activate PMS and remove 95.2% FF within 40 min. After loading $CoFe_2O_4$ onto eggshell surface, with the increase of eggshell content (mass ratio), FF degradation efficiency in $CoFe_2O_4$/eggshell and PMS system first increased, and then decreased. The reason for this phenomenon might be that when $CoFe_2O_4$ nanoparticles were loaded on eggshell, the size of $CoFe_2O_4$ nanoparticles would become smaller and more dispersed, which could be conducive to the contact between PMS and active sites, thus improving the degradation efficiency of FF. However, when eggshell mass ratio increased (which corresponded to a decrease of $CoFe_2O_4$ mass ratio), the total active sites decreased, which in turn led to the decrease in FF removal efficiency. Among them, the composite with 40% eggshell mass ratio could reach the highest PMS catalytic activity and degraded 96.8% FF in 40 min, and corresponding HPLC spectra during FF degradation are shown in the Fig. 2. Therefore, the composites with an eggshell mass ratio of 40% were chosen for subsequent experiments in this study, and all subsequent references to $CoFe_2O_4$/eggshell in this paper refer to the composites with an eggshell mass ratio of 40%.

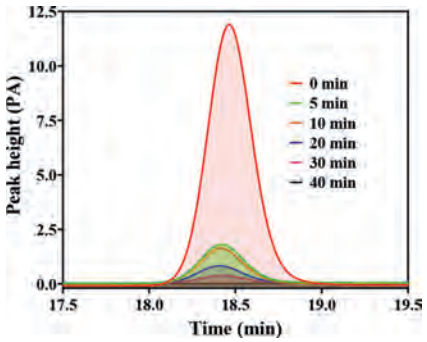

Fig. 2. HPLC spectra of FF degradation by $CoFe_2O_4$/eggshell (40%) and PMS system. Experimental conditions: [PMS] = 0.96 mmol/L, [Catalyst] = 0.4 g/L, [FF] = 10 mg/L.

TOC is usually used to describe the mineralization efficiency in containment oxidative degradation system. As described in Fig. S7b (Supporting information), in $CoFe_2O_4$/eggshell and PMS system, TOC concentration increased significantly in the first 5 min, which might be due to the dispersion of carbon content from eggshell into solution. Then, TOC values decreased gradually with the degradation process, which indicated that the PMS and the radicals released from the PMS activation period further mineralized organic substance in the solution. In 40 min, TOC concentration in the system accounted for 57.0% of the original TOC concentration. At the same time, the residual concentration of PMS was also examined to characterize consumption rate of PMS, and 42.3% (5 min), 53.8% (10 min), 68.6% (20 min), 70.7% (30 min) and 71.0% (40 min) of PMS were consumed. As shown in Fig. S7b, consumption of PMS increased slowly after 20 min, which was also consistent with the variation pattern of the degradation efficiency of FF with the reaction time.

Dosage of PMS played a crucial job in FF degradation process on account of the generation of high active radicals during PMS activation process. Various control experiments were conducted to further explore the effect of the PMS dosage in $CoFe_2O_4$/eggshell and PMS system towards FF degradation and the results were illustrated in Fig. S8a (Supporting information). The study on the effect of PMS dosage on FF degradation at the concentration of 0.32–1.6 mmol/L was also included. With PMS dosage increased to 1.6 mmol/L, FF degradation rate continually increased from 54.7% to 97.2% in 120 min, which was because of the increase of PMS concentration accelerating the formation of active radicals. When

dosage of PMS raised from 0.32 mmol/L to 0.64 mmol/L, degradation efficiency and reaction constant increased synchronously. However, in the interval of dosing from 0.64 mmol/L to 1.6 mmol/L, the increment of these two data boosts was significantly reduced. This might be that the utilization rate of active sites on the catalyst surface had tended to saturation and PMS dosage had played a critical role during the process when the PMS dosage is low, while the influence of PMS on oxidation process decreased with the increase of PMS dosage. Evidently, the elimination process of FF mainly concentrated in the first 40 min. Comprehensively, to save the reaction time and cost and improve the reaction efficiency, our group set the PMS dosage of 0.96 mmol/L and 1.28 mmol/L for further optimization experiment and set the reaction time as 40 min.

Concentration of catalysts was an important factor affecting the organic pollutant elimination. Therefore, Figs. S8b and c (Supporting information) exhibited the degradation efficiencies of FF on various catalysts concentrations (0.1–0.8 g/L) with the PMS dosage is 0.96 mmol/L or 1.28 mmol/L. As presented in Fig. S8b and c, since the concentrations of $CoFe_2O_4$/eggshell ranged from 0.1 g/L to 0.8 g/L, FF removal rate raised to 96.9% with 1.28 mmol/L PMS. Meanwhile, when the dosage of PMS is 0.96 mmol/L, the degradation rate kept increasing from 64.1% to 96.8% as concentrations of catalysts raised to 0.4 g/L. However, while the concentration of catalysts was added to 0.6 g/L and 0.8 g/L, it exhibited a slight decline in FF degradation efficiency compared with 0.96 mmol/L PMS. Seen from previous research reports, this phenomenon might be attributed to the scavenging effect due to excessive catalysts input [34]. Thus, 0.4 g/L catalysts and 0.96 mmol/L PMS were chosen as the optimal reaction conditions to eliminate FF in subsequent experiments.

It is known that AOPs based on PMS activation to degrade contaminants would be affected by the initial pH values of the system. Therefore, the removal efficiency of FF in $CoFe_2O_4$/eggshell and PMS system with different initial pH values of 2, 4, 9 and 11 was investigated. Meanwhile, the degradation efficiency of FF in this system at the original pH (pH 6.61) was also investigated for comparison, and results were shown in Fig. S8d (Supporting information). Through data analysis, it could be found that the change of initial pH of the solution had limited effect on removal efficiency of FF. Under the condition that initial pH value was not adjusted, the oxidation degradation efficiency of FF could reach the highest (96.8%) after 40 min. And with the initial pH at 2, the removal rate of FF could still reach 86.4%. When initial pH was under acidic condition, the oxidative degradation efficiency of FF in $CoFe_2O_4$/eggshell and PMS system decreased as the acidity increased, which might be attributed to the ability of the widely present H^+ in the solution to scavenge the $SO_4^{\bullet-}$ and $^{\bullet}OH$ radicals in the system under acidic conditions [35]. On the other hand, acidic solution would corrode $CoFe_2O_4$/eggshell composites and damage the structure of catalytic materials thereby reducing the efficiency in activating PMS and ultimately reducing the degradation efficiency of FF. When the system's initial pH was under alkaline conditions, FF removal efficiency decreased with the raise of alkalinity. When system's initial pH value was 9, FF degradation rate was 92.4% in 40 min, while it was 11, removal rate of FF was 87.3%. This phenomenon was because of system's initial pH value had determined the existing form of PMS. According to the literature [36], PMS has two pK_a values, < 0 and 9.4, respectively. This means that when the pH of the solution is greater than 9.4, the main existing form of PMS in the aqueous solution is SO_5^{2-}, and its reaction activity is much lower than that of HSO_5^-, so the proportion of SO_5^{2-} in the system of pH 9 is lower than that of the system of pH 11. Therefore, the more alkaline the system was, the less HSO_5^- could be activated to produce reactive radicals [37], which led to the decrease in FF degradation efficiency. In addition, the lifespan of $SO_4^{\bullet-}$ and $^{\bullet}OH$ radicals would decrease under alkaline conditions, resulting in insufficient concentration of radicals to diffuse into the solution and contact with pollutants for oxidative degradation. Apart from these, the pH change as the reaction progresses was recorded in Fig. S9 (Supporting information). In summary, $CoFe_2O_4$/eggshell and PMS system had a higher tolerance to initial pH of the solution. Under the original pH condition (6.61), the degradation rate of FF was the highest, but with the increase of acidity and alkalinity, FF degradation rate slightly decreased.

To investigate the influence of system temperature on FF degradation, this study recorded the degradation rate of FF in $CoFe_2O_4$/eggshell and PMS system under different temperatures by adjusting the reaction temperature inside the thermostatic oscillator. The results were exhibited in Fig. S8e (Supporting information). Obviously, although the degradation rate of FF could already reach 92.6% at the system temperature of 10 °C, the degradation rate of FF could still be significantly improved with the increasing of the system temperature, which indicated that the temperature plays a facilitating role in the reaction. This was because temperature could not only promote the activation efficiency of PMS, but also accelerate the collision frequency between molecules on the surface of catalytic materials [38].

To test the practicality of this system in real water, which contains many ions and organic matter, the influence of co-existing anions and organic matter in the solution system on FF elimination was investigated. By adding several typical co-existing anions (*e.g.*, Cl^-, HCO_3^-, NO_3^- and $H_2PO_4^-$) and humic acid (HA) to the target containment solution with different concentrations, the removal efficiency of FF was recorded at regular intervals by quantitatively adding catalyst and PMS to subsequently initiate the reaction, and the results were present in Figs. S8f–j (Supporting information). Fig. S8f exhibited FF removal efficiency in the system after adding 5, 10, and 50 mmol/L Cl^- into the system. Compared with the system without Cl^-, the degradation rate of FF at 40 min decreased rapidly to 24.61% after the addition of 5 mmol/L Cl^-. With concentration of Cl^- was added to 10 mmol/L, FF elimination rate at 40 min decreased to 17.46%. This phenomenon was because the addition of Cl^- would consume PMS, radicals ($SO_4^{\bullet-}$ and $^{\bullet}OH$) and produce less active Cl_2 [39], the process was shown in Eqs. 1–8. However, with concentration of Cl^- raised to 50 mmol/L, compared with the systems containing 5 mmol/L and 10 mmol/L Cl^-, the oxidation degradation efficiency of FF increased significantly, reaching 82.5% in 40 min, but still lower than 96.8% in the system without Cl^-. This might be because with the increase of Cl^- concentration, sufficient Cl^- concentration could ensure the formation of relatively high active $Cl^{\bullet}$ and $Cl_2^{\bullet-}$ [40] and thus relatively promoted the degradation of FF. And Cl^- would still consume PMS, $SO_4^{\bullet-}$ and $^{\bullet}OH$, which led to a still lower degradation efficiency of FF compared to the system without the introduction of Cl^-.

$$SO_4^{\bullet-} + Cl^- \rightarrow SO_4^{2-} + Cl^{\bullet},\ k = (3.2 \pm 0.2) \times 10^8\ \text{L mol}^{-1}\ \text{s}^{-1} \quad (1)$$

$$Cl^- + C \rightarrow Cl_2^{\bullet-} \quad (2)$$

$$Cl^{\bullet} + Cl^{\bullet} \rightarrow Cl_2 \quad (3)$$

$$Cl_2^{\bullet-} + Cl_2^{\bullet-} \rightarrow Cl_2 + 2Cl^- \quad (4)$$

$$^{\bullet}OH + Cl^- \rightarrow HOCl^{\bullet-},\ k = (2.6 \pm 0.6) \times 10^8\ \text{L mol}^{-1}\ \text{s}^{-1} \quad (5)$$

$$HOCl^{\bullet-} + H^+ \rightarrow Cl^- + H_2O \quad (6)$$

$$HSO_5^- + Cl^- \rightarrow SO_4^{2-} + HOCl \quad (7)$$

$$HSO_5^- + 2Cl^- + H^+ \rightarrow SO_4^{2-} + H_2O + Cl_2 \quad (8)$$

CO_2 is one of the important components of air, and it can form bicarbonate after dissolving in water, thus HCO_3^- is often widely present in nature water. Fig. S8g exhibited the influence of introducing 5 mmol/L, 10 mmol/L and 50 mmol/L HCO_3^- into the system on FF degradation efficiency. It could be observed that various dosage of HCO_3^- would inhibit the removal of FF in $CoFe_2O_4$/eggshell and PMS system. With the increase of HCO_3^- concentration to 50 mmol/L, FF degradation rate decreased from 41.74% to 7.46%, which is consistent with previous report [41], which interpreted this phenomenon as the scavenging effect of HCO_3^- on $SO_4^{\bullet-}$ and $^{\bullet}OH$. According to a previous study [42], NO_3^- could also have a scavenging effect on $SO_4^{\bullet-}$ and $^{\bullet}OH$ radicals, generating less reactive radicals and thus weakening the degradation of FF in this system, as shown in Fig. S8h. According to Fig. S8i, the addition of $H_2PO_4^-$ exhibited a more pronounced negative effect on the degradation of FF, and the inhibitory effect intensified with the increase of $H_2PO_4^-$ concentration. The reason for this phenomenon could be the conversion of $SO_4^{\bullet-}$ and $^{\bullet}OH$ and the generation of radicals with weaker oxidation capacity (as shown in Eqs. 9 and 10. In addition, $H_2PO_4^-$ also has strong affinity with some transition metals and can bind with some transition metals, thus weakening its activation effect on PMS [43].

$$SO_4^{\bullet-} + H_2PO_4^- \rightarrow SO_4^{2-} + H_2PO_4^{\bullet-} \quad (9)$$

$$^{\bullet}OH + H_2PO_4^- \rightarrow OH^- + H_2PO_4^{\bullet-} \quad (10)$$

The macromolecule humic acid (HA) is usually a complex organic substance formed by physical, chemical, and biological action of animal or plant residues over a long period of time. It could be observed from Fig. S8j that after HA was introduced into the system, degradation reaction was slightly inhibited in the first 20 min, and this inhibition effect increased with the increase of HA dosage. This was because HA could not only compete with the radicals in aqueous solution [44], but also had a strong π-π bond stacking effect thus obscuring the active site of the catalytic material leading to weakened activation of the material [45]. However, all experimental groups added with HA could still obtain relatively high FF removal efficiency at 40 min, and inhibition effect of HA concentration on final FF removal efficiency was not significant. This was because a great quantity of radicals was released continuously during PMS activation, which might partially degrade HA in the first 20 min and retarded the inhibition effect of HA in second half of the reaction.

For validating the practical application of $CoFe_2O_4$/eggshell and PMS system, the effects of five different water matrices, which include lake water, river water, tap water, industrial wastewater, and ultra-pure water, on the elimination efficiency of FF was evaluated. Some of the water quality indicators for different water matrices were listed in Table S1 (Supporting information). Corresponding removal data were plotted as in Fig. S10 (Supporting information), which exhibited that the removal efficiency of FF by $CoFe_2O_4$/eggshell and PMS system in ultrapure water (96.8%) was much higher than that of river water (37.8%), tap water (34.4%), lake water (30.6%) and industrial wastewater (22.7%). The alkalinity, TOC, and natural constituents in water body, including natural organic matter (NOM) and dissolved organic matters (DOM) [46], could show adverse influence on FF degradation. In addition, natural colloidal particles (NCPs) with particle sizes in range of 1 nm~1μm, which widely disturbed in natural water body [47], could also contribute to the inhibition effect. Therefore, the degradation efficiency of FF would be inhibited in natural waters such as lake water and river water. Meanwhile, owing to higher alkalinity of the lake water, FF degradation efficiency in lake water would be easier to be inhibited than that in river water [47]. Moreover, the inhibition of FF degradation rate in tap water may come from disinfectants and their by-products, such as hypochlorite (HClO). The industrial wastewater we used for the experiment is petrochemical wastewater from Lanzhou Petrochemical Company in Gansu Province. The lowest removal efficiency (22.72%) was achieved in the reaction conducted in petrochemical wastewater, which could likely be ascribed to the existence of higher concentration of total nitrogen, chemical oxygen content, and hydrocarbons, chlorinated chemicals [48].

Degradation of contaminants in aqueous solutions by heterogeneous activated PMS is a complex process during which various radicals will be generated, including $SO_4^{\bullet-}$ and $^{\bullet}OH$, *etc.* In order to identify the reactive radicals produced during the degradation of FF by $CoFe_2O_4$/eggshell and PMS system, electron parametric resonance (EPR) method was adopted and the results were present in Fig. 3. Clear characteristic peaks of DMPO-$^{\bullet}OH$ could be observed in Fig. 3a [49], but it is difficult to discern the presence of the characteristic peaks of DMPO-$SO_4^{\bullet-}$ and DMPO-$O_2^{\bullet-}$. This phenomenon suggested that $CoFe_2O_4$/eggshell was able to efficiently activate PMS and release a large amount of $^{\bullet}OH$. To verify the presence of $O_2^{\bullet-}$ in the system, EtOH was added to the reaction system to quench the $SO_4^{\bullet-}$ and $^{\bullet}OH$ radicals in the system, and samples were taken and tested by EPR, the results of which were shown in Fig. 3b, where the spurious peaks appeared in the graph. The weakened characteristic peak belonging to DMPO-$^{\bullet}OH$ was identified at the same position in Fig. 3b according to the position of the DMPO-$^{\bullet}OH$ characteristic peaks from Fig. 3a, and sixfold peaks of DMPO-$O_2^{\bullet-}$ was also identified, which indicates the presence of $O_2^{\bullet-}$ in the system. Meanwhile, EPR test using TEMP as spin-trapping regent was also performed, and as shown in Fig. 3c, a triple peak of TEMP-$^1O_2$ was observed [49], and it could be concluded that $^1O_2$ was also generated during the reaction.

To determine the contribution of various free radicals to the degradation of FF in the $CoFe_2O_4$/eggshell and PMS system, methanol (MeOH) and *tert*-butanol (TBA) were mixed into the system for radical quenching experiments. The reaction rate constant for the scavenging effect of TBA on the $SO_4^{\bullet-}$ are about (4–9.1) $\times$ 10^5 L mol^{-1} s^{-1}, while reaction rate constant for the elimination effect on $^{\bullet}OH$ is about (3.8–7.6) $\times$ 10^8 L mol^{-1} s^{-1}, so TBA can be used to inhibit $^{\bullet}OH$, while MeOH can effectively scavenge $SO_4^{\bullet-}$ and $^{\bullet}OH$ radicals [50,51]. From Fig. 3d, FF removal efficiency was significantly inhibited in all $CoFe_2O_4$/eggshell and PMS systems with the addition of 10–100 mmol/L MeOH and TBA. The removal efficiency of FF was lower than 9% in all groups, and inhibition effect caused by MeOH was slightly stronger than that by TBA. In all the groups added with MeOH, FF hardly degraded. In addition, sodium azide (NaN_3), which mainly shows active toward $^1O_2$ ($k = 1.0 \times 10^9$ L mol^{-1} s^{-1}) [52], had been used as quenchers to determine the contribution of $^1O_2$ to FF removal. Fig. 3d revealed that FF degradation was barely inhibited by the addition of 1 mmol/L NaN_3, and FF removal efficiency hardly increased or decreased after increasing the concentration of NaN_3. This illustrated that NaN_3 has no inhibitory effect on FF degradation in this system, and the role of $^1O_2$ could be ignored, which was corresponded with previous report [53]. By comparing the difference in the efficiency of FF degradation between the systems with the addition of TBA and MeOH at the same concentration, it could be concluded that $^{\bullet}OH$ played a major role in the system of $CoFe_2O_4$/eggshell and PMS, while $SO_4^{\bullet-}$ only played an auxiliary role.

Polyvinylidene fluoride (PVDF) membranes were synthesized to reduce the metal release from $CoFe_2O_4$/eggshell. The surface morphology of $CoFe_2O_4$/eggshell PVDF membrane was analyzed by scanning electron microscopy (SEM). As shown in Fig. S11 (Supporting information), the existence of pores on the membrane

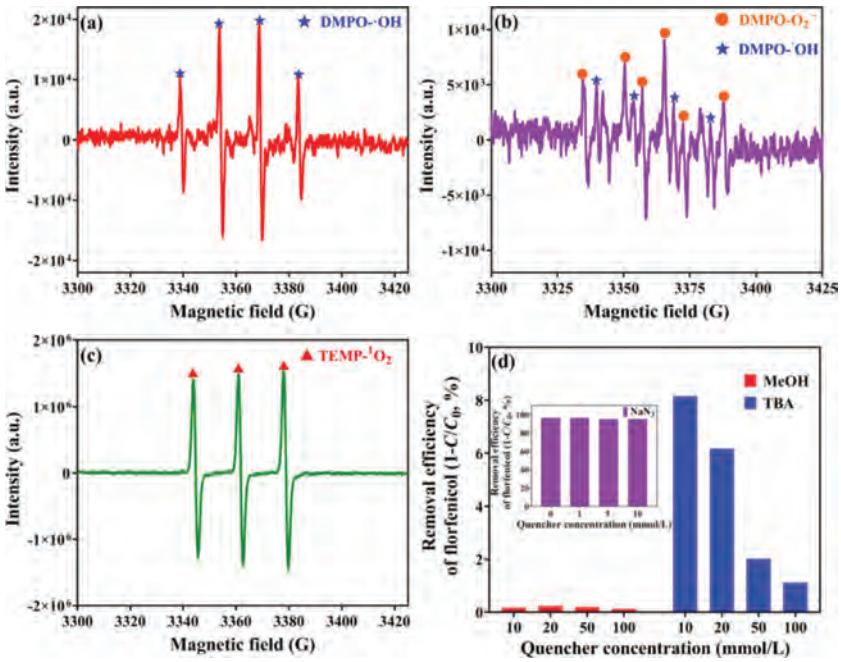

Fig. 3. EPR spectra in various reactions using DMPO (a, b) and TEMP (c) as spin-trapping regent, FF degradation in PMS activation system in presence of various scavengers (d). Experimental conditions: [Catalyst] = 0.4 g/L, [PMS] = 0.96 mmol/L, [FF] = 10 mg/L.

surface could be clearly observed. Energy dispersive spectrometer (EDS) analysis was also performed (Fig. S12 in Supporting information), which could clearly show that F, C, O, Ca, Fe and Co coexistence in the $CoFe_2O_4$/eggshell PVDF membrane, indicating that the $CoFe_2O_4$/eggshell PVDF membrane had been successfully synthesized. Content of F and C was high, while content of Co and Fe and Ca was low, which revealed that most of the components in the membrane are PVDF substrate and the powder catalyst was encapsulated within the PVDF substrate. In addition, the structures of $CoFe_2O_4$/eggshell, PVDF membrane and $CoFe_2O_4$/eggshell PVDF membrane were tested by X-ray diffraction (XRD) method, and the data were shown in Fig. S13 (Supporting information). We could observe that the XRD spectrum of the pure PVDF membrane in Fig. S13 was consistent with the results of the relevant literature [54], proving the high purity of the synthesized PVDF membrane. However, the XRD pattern of $CoFe_2O_4$/eggshell PVDF membrane had no obvious characteristic peaks of $CoFe_2O_4$ and $CaCO_3$, which might be related to the low relative content of $CoFe_2O_4$/eggshell in the membrane [55]. It is well known that the stability and reusability of the catalytic materials used to activate PMS for the degradation of pollutants are the key indicators for the evaluation of catalytic materials. The specific operation of repeated experiment could be viewed in Text S5 (Supporting information). In this study, cycle experiments of $CoFe_2O_4$/eggshell and PMS system were conducted for 7 times, and data were shown by Fig. S14 (Supporting information). Composites were reclaimed through centrifugal separation method, washed by ethanol and ultra-pure water for several alternating repetitions, and finally placed in an oven for drying, with the temperature adjusted to 60 °C. The cycle experiments were carried out under the same experimental conditions. It could be observed from the Fig. S14 that degradation efficiency of FF in 7 cycles of $CoFe_2O_4$/eggshell and PMS system in 40 min are 96.8%, 90.9%, 91.0%, 91.1%, 89.9%, 89.0% and 88.1%, respectively. The degradation efficiency in the cyclic experiments first decreased significantly, which might be because of metal's precipitation, adsorption of intermediates on surface and the destruction of the composite. The degradation efficiency afterwards slightly increased in the 3rd and 4th cycling experiments, which might be due to the destruction of the composite surface thus leading to the shedding of the adsorbed intermediates and partial exposure of the active sites, thus increasing the degradation rate. The degradation rate decreased again in the 5th–7th cycle experiments, which might be due to the further destruction of eggshell in the catalytic material and the aggregation of the exposed $CoFe_2O_4$ nanoparticles on the surface. In order to further observe the microstructure after reaction, the SEM image of $CoFe_2O_4$/eggshell after 7 times repeated experiment was displayed in Fig. S15 (Supporting information). It could be observed that the eggshell had been corroded to some extent, but $CoFe_2O_4$ nanoparticles were still loaded on the surface of eggshell in a small form, and there was no agglomeration. This could ensure full contact between the active site of $CoFe_2O_4$ nanoparticles and PMS. Meanwhile, the reusability and stability of $CoFe_2O_4$/eggshell PVDF membrane were also tested. As we could see from Fig. S14, FF removal efficiency in $CoFe_2O_4$/eggshell PVDF membrane and PMS system were 91.3%, 90.8%, 90.9%, 91.2%, 90.8%, 89.8% and 89.7%, respectively. After 7 cycles, the removal efficiency of FF in $CoFe_2O_4$/eggshell PVDF Membrane and PMS system decreased by 1.6%, which was much lower than that in $CoFe_2O_4$/eggshell and PMS system by 8.7%, which indicated that the PVDF membrane was more stable than the catalyst powder. At the same time, the leaching amounts of Fe and Co in $CoFe_2O_4$ and PMS system were 0.0257 mg/L and 0.0320 mg/L, respectively. The leaching amounts of Fe and Co in $CoFe_2O_4$ and PMS system were 0.0036 mg/L and 0.0044 mg/L. But the leaching amounts of Fe and Co in $CoFe_2O_4$/eggshell PVDF Membrane and PMS system were only 0.0013 and 0.0017 mg/L, which are far lower than the former two systems. It can be demonstrated that encapsulating $CoFe_2O_4$/eggshell in PVDF membrane could not only enhance the stability and reusability of the composite catalytic material, but also control the metal precipitation.

In this study, variation of the microbial toxicity during the activated oxidative degradation of FF by PMS was investigated using the activated sludge inhibition method. As can be observed from Fig. S16 (Supporting information), the initial FF solution (10 mg/L) could inhibit oxygen absorption by about 60.0%. With the degradation of FF, inhibition rate of oxygen absorption obviously de-

creased, indicating that FF was further degraded and mineralized during the process with its intermediates, and the final inhibition rate of oxygen absorption decreased to about 25.0%. It should be noted that decrease degree of oxygen absorption inhibition rate in the first 10 min was significantly faster than that in the later reaction period, which may be due to the decrease of the degradation rate of FF intermediates because of the increase of intermediates' concentration in this system. To further investigate the degradation pathway of FF in this system, the intermediate products during the FF removal process were detected by LC-MS method. Based on the analysis of products' fragment spectra and relative molecular masses of deprotonated molecules, the possible degradation pathways of FF could be determined in Fig. S17 (Supporting information). The evolution of FF during the activation of PMS by $CoFe_2O_4$/eggshell for FF degradation was very complicated. Broadly, it could be divided into three types of pathways: (1) Dehalogenation and/or hydroxylation, then hydrolysis of amide bond, and then further oxidative degradation, (2) hydroxylation of fluorine, then dehalogenation, followed by hydrolysis of amide bond, (3) direct hydrolysis and then dehalogenation. Following these pathways, the products might further undergo dehalogenation, defluorination, desulfurization, and oxidation reactions to produce carbon dioxide, water, and small molecules. Partial or complete dehalogenation and cleavage of C–F bond during FF degradation could effectively reduce the antibiotic resistance and toxicity of FF [56]. It could be observed from Fig. S17 that most of the degradation paths had achieved the purpose of dehalogenation and defluorination, which also reflected the phenomenon that the toxicity of the reaction process effectively decreased with the reaction time. At the same time, the defluorination efficiency was also monitored. Fig. S18 (Supporting information) showed that defluorination efficiency in this system continued to increase with the progress of the reaction, and it could reach 74.8% in 40 min, which was lower than the FF removal efficiency. This might be the reason that some of small-molecular intermediates containing fluorine hadn't been further and completely degraded during the degradation process.

In this study, the active radicals produced through the process of PMS activation by $CoFe_2O_4$/eggshell were identified by the EPR tests combined with radicals quenching experiments. It was confirmed that $^{\bullet}OH$ and $SO_4^{\bullet-}$ were the main radicals involved in the degradation of FF in $CoFe_2O_4$/eggshell and PMS system. In order to better understand the catalytic mechanism of FF removal in $CoFe_2O_4$/eggshell and PMS system, XPS method was carried out to compare the difference between fresh and used $CoFe_2O_4$/eggshell, as shown in Fig. S4. According to the data, it could be observed that the fine spectra of O 1s and Ca 2p in the $CoFe_2O_4$/eggshell catalytic material exhibited little difference before and after 7 cycles of experiments, while the fine spectra of Fe 2p and Co 2p show more obvious changes. The XPS spectra of Fe 2p in the $CoFe_2O_4$/eggshell composites before reaction can be divided into Fe(II) and Fe(III), whose contents were 47.2% and 52.8%, respectively, according to the integrated area of the spectra. And after the reaction, relative content of Fe(II) decreases to 43.7%, while relative content of Fe(III) increases to 56.3%. Meanwhile, after reaction, relative content of Co(II) in the composites decreased from 62.2% to 59.6%, and relative content of Co(III) in the composites raised from 37.8% to 40.4%. And from the C 1s fine spectrogram of the fresh and used $CoFe_2O_4$/eggshell composites could be observed that the content of CO_3^{2-} decreases from 22.6% to 14.9%, which indicated that the eggshell structure in the composites had been destroyed and decomposed during the reaction. The above analysis revealed that Fe(II) and Co(II) played a key role in the activation of PMS by $CoFe_2O_4$/eggshell composites to degrade FF, and they were the main contributors to the activation of HSO_5^-, resulting in abundant $^{\bullet}OH$ and $SO_4^{\bullet-}$. According to the hypothesis described in the paper

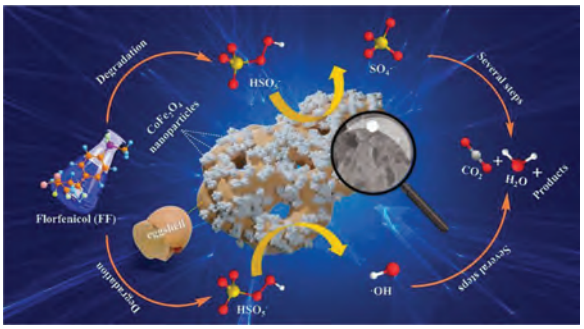

Fig. 4. Proposed mechanism for the catalytic FF oxidation over the by $CoFe_2O_4$/eggshell and PMS system.

published by academician Ma Jun of Harbin Institute of Technology [10], metal ions could play the role of Lewis sites to bind with H_2O molecules, thus promoting the formation of active species on cobalt ferrite's surface by a large number of hydroxyl groups, as shown in Eq. 11. PMS could also bind with cobalt-iron oxides *via* hydroxyl groups in solution, and in this structure, cobalt would act as an active site to transfer electrons. Electrons could be transferred by Co(II)-Co(III) to activate PMS and promote the fracture of H–O and O-O bonds, then producing $SO_4^{\bullet-}$ and $SO_5^{\bullet-}$, as shown in Eqs. 12–14 [57], and $SO_5^{\bullet-}$ could be further converted to $SO_4^{\bullet-}$, $SO_4^{\bullet-}$ could also react with H_2O or OH^- to form $^{\bullet}OH$. In addition, PMS could also generate reactive radical species such as $SO_5^{\bullet-}$ and $SO_4^{\bullet-}$ through Fe(III) activation on the surface of cobalt-iron oxides, as shown in Eqs. 15 and 16 [13]. After that, as shown in Eq. 17, the oxidative degradation of FF was carried out by $SO_4^{\bullet-}$ and $^{\bullet}OH$ produced by the above reaction. The process of FF degradation by $CoFe_2O_4$/eggshell activated PMS was roughly shown in Fig. 4.

$$\equiv Co^{2+} + H_2O \rightarrow \equiv Co^{2+} - OH + H^+ \quad (11)$$

$$\equiv Co^{2+} - OH + HSO_5^- \rightarrow \equiv CoO^+ + SO_4^{\bullet-} + H_2O \quad (12)$$

$$\equiv CoO^+ + H^+ \rightarrow \equiv Co^{3+} + H_2O \quad (13)$$

$$\equiv Co^{3+} + HSO_5^- \rightarrow \equiv Co^{2+} + SO_5^{\bullet-} + H^+ \quad (14)$$

$$\equiv Fe^{3+} + HSO_5^- \rightarrow \equiv Fe^{2+} + SO_5^{\bullet-} + H^+ \quad (15)$$

$$\equiv Fe^{2+} + HSO_5^- \rightarrow \equiv Fe^{3+} + SO_4^{\bullet-} + H_2O \quad (16)$$

$$^{\bullet}OH,\ SO_4^{\bullet-} + FF \rightarrow \text{severalsteps} \rightarrow CO_2 + H_2O + \text{products} \quad (17)$$

The $CoFe_2O_4$/eggshell composites were prepared by a simple and convenient hydrothermal synthesis method. After loading on the eggshell surface, the size and agglomeration of $CoFe_2O_4$ nanoparticles were controlled and distributed irregularly on the eggshell surface and in the pores. By optimizing the catalysts dosage and the initial concentration of PMS, it was demonstrated that total elimination rate of FF can reach 96.8% within 40 min in the system with $CoFe_2O_4$/eggshell (0.4 g/L) and PMS (0.96 mmol/L). Besides, batch of control experiments with different operation parameters and water matrices demonstrated the validity of the $CoFe_2O_4$/eggshell to remove FF under various conditions. The radicals in the reaction process were identified by EPR tests, and the radical quenching experiments confirmed that $SO_4^{\bullet-}$ and $^{\bullet}OH$ played a dominant role during the FF degradation process. Based on these data, a possible mechanism for FF degradation in this

system was proposed. Through activated sludge inhibition experiments, it was found that the toxicity within the system decreased as the reaction proceeded. The intermediates of FF were measured, and it was found that both dehalogenation and defluorination were effectively carried out during the degradation of FF. The $CoFe_2O_4$/eggshell composites were loaded on the PVDF membrane by the scraping method, which effectively improved the stability of the material and controlled the metal precipitation.

Declaration of competing interest

We have no conflicts of interest to declare.

Acknowledgments

This work was kindly funded by National Natural Science Foundation of China (No. 51978319), Outstanding Youth Foundation of Gansu Province (No. 20JR10RA651), Natural Science Foundation of Gansu Province (No. 20JR5RA242 and 20JR10RA635) and Natural Science Project of University Research Program of Xinjiang Uygur Autonomous Region (No. XJEDU2017M035).

Supplementary materials

Supplementary material associated with this article can be found, in the online version, at doi:10.1016/j.cclet.2021.11.096.

References

[1] Q. Zhao, Y. Wang, S. Wang, et al., Sci. Rep. 6 (2016) 32192.
[2] Y. Chen, S. Lan, M. Zhu, Chin. Chem. Lett. 32 (2021) 2052–2056.
[3] W.L. Jiang, X. Xia, J.L. Han, et al., Environ. Sci. Technol. 52 (2018) 9972–9982.
[4] N. Liu, S. Sijak, M. Zheng, et al., Chem. Eng. J. 260 (2015) 826–834.
[5] P. Ding, J. Niu, F. Chang, et al., Chin. Chem. Lett. 32 (2021) 2495–2498.
[6] S. Guo, H. Tang, L. You, et al., Chin. Chem. Lett. 32 (2021) 2828–2832.
[7] H.B. Qiu, P.C. Guo, L. Yuan, G.P. Sheng, Chin. Chem. Lett. 31 (2020) 2614–2618.
[8] G.P. Anipsitakis, E. Stathatos, D.D. Dionysiou, J. Phys. Chem. B 109 (2005) 13052–13055.
[9] K. Shih, T. White, J.O. Leckie, Environ. Sci. Technol. 40 (2006) 5520–5526.
[10] Y. Ren, L. Lin, J. Ma, et al., Appl. Catal. B 165 (2015) 572–578.
[11] Z. Yang, Y. Li, X. Zhang, et al., Chem. Eng. J. 384 (2020) 123319.
[12] D. Espino, Y. Haruvy-Manor, Y. Mastai, J. Polym. Environ. 27 (2019) 827–836.
[13] Y. Tan, C. Li, Z. Sun, et al., Chem. Eng. J. 388 (2020) 124386.
[14] X. Li, X. Liu, C. Lin, et al., Chem. Eng. J. 367 (2019) 208–218.
[15] C. Liu, L. Chen, D. Ding, T. Cai, Appl. Catal. B 254 (2019) 312–320.
[16] J. Wu, G. Cagnetta, B. Wang, et al., Chem. Eng. J. 368 (2019) 824–836.
[17] E. Mosaddegh, F.A. Hosseininasab, A. Hassankhani, RSC Adv. 5 (2015) 106561–106567.
[18] A. Laca, A. Laca, M. Díaz, J. Environ. Manag. 197 (2017) 351–359.
[19] J. Liu, J. Shen, M. Li, L.P. Guo, Chin. Chem. Lett. 26 (2015) 1478–1484.
[20] H. Pang, C. Wei, X. Li, et al., Sci. Rep. 4 (2014) 3577.
[21] J. Liu, R. Meng, J. Li, et al., Appl. Catal. B 254 (2019) 214–222.
[22] X. Zhang, M. Liu, Z. Kang, et al., Chem. Eng. J. 388 (2020) 124304.
[23] J. Wang, B. Xiong, L. Miao, et al., Appl. Catal. B 280 (2021) 119422.
[24] X. Ma, X. Feng, J. Guo, et al., Appl. Catal. B 147 (2014) 666–676.
[25] S. Guo, H. Wang, W. Yang, et al., Appl. Catal. B 262 (2020) 118250.
[26] H. Zhang, C. Li, L. Lyu, C. Hu, Appl. Catal. B 270 (2020) 118874.
[27] W. Wu, D. Tian, T. Liu, et al., Chem. Eng. J. 394 (2020) 124938.
[28] R. Foroutan, M. Ahmadlouydarab, B. Ramavandi, R. Mohammadi, J. Environ. Chem. Eng. 6 (2018) 6049–6058.
[29] Y. Guo, D.P. Yang, M. Liu, et al., J. Mater. Chem. A 7 (2019) 8832–8844.
[30] A.R. Gupta, V.K. Rathod, Waste Manag. 79 (2018) 169–178.
[31] S. Dash, S. Das, M.I. Khan, et al., Mater. Chem. Phys. 220 (2018) 409–416.
[32] S. Mirzaei, V. Javanbakht, Int. J. Biol. Macromol. 134 (2019) 1187–1204.
[33] M. Nasrollahzadeh, S.M. Sajadi, A. Hatamifard, Appl. Catal. B 191 (2016) 209–227.
[34] R. Zhang, M. Chen, Z. Xiong, Y. Guo, B. Lai, Chin. Chem. Lett. 33 (2022) 948–952.
[35] M. Ahmadi, F. Ghanbari, Environ. Sci. Pollut. Res. 25 (2017) 6003–6014.
[36] M. Ma, L. Chen, J. Zhao, W. Liu, H. Ji, Chin. Chem. Lett. 30 (2019) 2191–2195.
[37] C. Li, J. Wu, W. Peng, Z. Fang, J. Liu, Chem. Eng. J. 356 (2019) 904–914.
[38] I. Othman, J. Hisham Zain, M. Abu Haija, F. Banat, Appl. Catal. B 266 (2020) 118601.
[39] P. Hu, M. Long, Appl. Catal. B 181 (2016) 103–117.
[40] H. Chen, Z. Zhang, M. Feng, et al., Chem. Eng. J. 313 (2017) 498–507.
[41] L. Kong, G. Fang, Z. Fang, et al., Chem. Eng. J. 416 (2021) 128996.
[42] J. Cao, L. Lai, B. Lai, et al., Chem. Eng. J. 364 (2019) 45–56.
[43] H. Zhou, L. Lai, Y. Wan, et al., Chem. Eng. J. 384 (2020) 123264.
[44] G. Chen, L.C. Nengzi, Y. Gao, et al., Chin. Chem. Lett. 31 (2020) 2730–2736.
[45] L. Chen, D. Ding, C. Liu, et al., Chem. Eng. J. 334 (2018) 273–284.
[46] C. Jiang, Y. Ji, Y. Shi, J. Chen, T. Cai, Water Res. 106 (2016) 507–517.
[47] M. Nie, C. Yan, X. Xiong, et al., Chem. Eng. J. 348 (2018) 455–463.
[48] C. Wu, Y. Zhou, Q. Sun, et al., J. Hazard. Mater. 309 (2016) 185–191.
[49] C. Lyu, L. Zhang, D. He, B. Su, Y. Lyu, Chin. Chem. Lett. 33 (2022) 930–934.
[50] S. Zhu, X. Li, J. Kang, X. Duan, S. Wang, Environ. Sci. Technol. 53 (2019) 307–315.
[51] M. Nie, Y. Deng, S. Nie, et al., Chem. Eng. J. 369 (2019) 35–45.
[52] P. Sun, H. Liu, M. Feng, et al., Appl. Catal. B 272 (2020) 119005.
[53] X. Lu, W. Qiu, J. Ma, et al., Chem. Eng. J. 401 (2020) 126128.
[54] Y. Zhang, L. Ye, W. Zhao, et al., J. Membr. Sci. 601 (2020) 117873.
[55] Y. Liu, R. Guo, G. Shen, et al., Chem. Eng. J. 405 (2021) 126990.
[56] D. Deng, F. Deng, B. Tang, J. Zhang, J. Liu, J. Hazard. Mater. 332 (2017) 168–175.
[57] X. Long, S. Yang, X. Qiu, et al., Chem. Eng. J. 404 (2021) 127052.